Colloidal Mie resonant silicon nanoparticles

Sugimoto, Hiroshi
Fujii, Minoru

(Citation)
Nanotechnology,32(45):452001

(Issue Date)
2021-08-19

(Resource Type)
journal article

(Version)
Accepted Manuscript

Colloidal Mie Resonant Silicon Nanoparticles

Hiroshi Sugimoto[1,2] and Minoru Fujii[1]

[1] Department of Electrical and Electronic Engineering, Graduate School of Engineering, Kobe University, Rokkodai, Nada, Kobe 657-8501, Japan
[2] JST-PRESTO, Honcho 4-1-8, Kawaguchi, Saitama 332-0012, Japan

E-mail: sugimoto@eedept.kobe-u.ac.jp

Received xxxxxx
Accepted for publication xxxxxx
Published xxxxxx

Abstract

Nano- and microstructures of silicon (Si) exhibit electric and magnetic Mie resonances in the optical regime, providing a novel platform for controlling light at the nanoscale and enhancing light–matter interactions. In this Review, we present recent development of colloidal Si nanoparticles (NPs) that have wide range of applications in nanophotonics. Following brief summary of synthesis methods of amorphous and crystalline Si particles with high sphericity, optical responses of single Si particles placed on a substrate are overviewed. Then, the capability as a nanoantenna to control light-matter interactions is discussed in different systems. Finally, collective optical responses of Si NPs in solution are presented and the application potentials are discussed.

Keywords: Mie resonance, colloid, silicon, nanoparticles

1. Introduction

Optically resonant nanostructures, that is often called “nanoantennas”, can manipulate light at the nanoscale and enable enhancement of local optical responses of nearby materials.[1,2] Localized surface plasmon resonances (LSPR) in noble metal nanostructures are the most widely utilized phenomena to realize a variety of nanoantennas that enhance Raman scattering,[3,4] fluorescence[5,6] and various nonlinear optical responses.[7,8]

The simplest plasmonic nanoantenna is a spherical metal nanoparticle (NP). Optical responses of a spherical particle is evaluated analytically using the Mie theory. A metal (real part of the permittivity (ε_r) < 0) sphere such as a gold (Au) or silver (Ag) particle with a size much smaller than the wavelength of light possesses only the lowest order electric dipole (ED) mode known as the Fröhlich mode,[9] and a larger one supports higher order electric multipole modes such as an electric quadrupole (EQ) mode. Resonant excitation of these electric modes enhances the electric field around a sphere significantly, inducing a variety of intriguing phenomena in photonics[10–13] and biophotonics.[14,15] A drawback of a plasmonic nanoantenna is the inevitable Joule heating under resonant excitation, which causes detrimental effects such as degradation of fluorescent dyes and biomolecules and limits the practical usage.

According to the Mie theory, a dielectric (ε_r>0) sphere has richer resonance behavior than the metal counterpart and Mie resonance of high refractive index dielectric NPs has been a subject of recent intensive studies. The revival of research on dielectric NPs was triggered by the demonstration of magnetic dipole (MD) resonance at the optical frequency.[16,17] Coexistence of ED and MD resonances in a nanostructure provides a powerful and unique platform for unprecedented control of light waves. Numerous photonic components utilizing the interference between the ED and MD modes have been proposed. Among high-index dielectrics having MD resonance in the visible range such as silicon (Si), germanium or gallium phosphide, [18–26] Si is most attractive because of the high-Q resonance due to the high refractive index and the small extinction coefficient in the visible range as well as the high compatibility to semiconductor industry, high environmental friendliness, earth abundance, etc. Highly developed Si nanofabrication technology enables us to fabricate Si-based Mie resonant metasurfaces composed of complicated nanostructures with very high accuracy.

Aside from the top-down processes for the production of Si-based Mie resonance devices, bottom-up processes have also been developed.[27] Free-standing Si NPs have been produced by several methods such as femtosecond laser ablation of bulk Si targets[16,17,28], mechanical grinding using a simple blender,[29] thermal disproportionation of Si suboxide, chemical vapor deposition, etc. In the bottom-up process, Si NPs are prepared in the powder form or dispersed in solution, or deposited directly on a substrate. Among them, the colloidal solution is most versatile, because it can be utilized for the production of higher-order structures via solution-based self-assembly approach. This approach meets the demand for the production of large-area and flexible nanophotonic devices with a lower cost. Unfortunately, solution-based bottom-up assembly of Si NPs is not very successful and is limited to very primitive structures.[30] This is mainly due to the lack of a high-quality colloidal solution. This situation is a large contrast to plasmonic NPs, where 1D to 3D structures have been produced from the colloidal solution with high accuracy.[31–34]

This Topical review provides recent progress on the development of colloidal Si NPs and microparticles that can be a precursor for self-assembled metasurfaces and metamaterials (Figure 1). Starting from brief summary of several production processes, optical responses of single Si NPs and fluorescence enhancement by Si NP nanoantennas are discussed. We then discuss optical responses of the colloidal solutions and the films produced from the solutions. We show that recent significant improvement of the quality of colloidal Si NPs makes Mie resonance behavior such as structural coloration and magnetic responses clearly observable in macroscopic samples composed of a huge number of Si NPs, and thus a new horizon is opening in the research on Si NP Mie resonators.

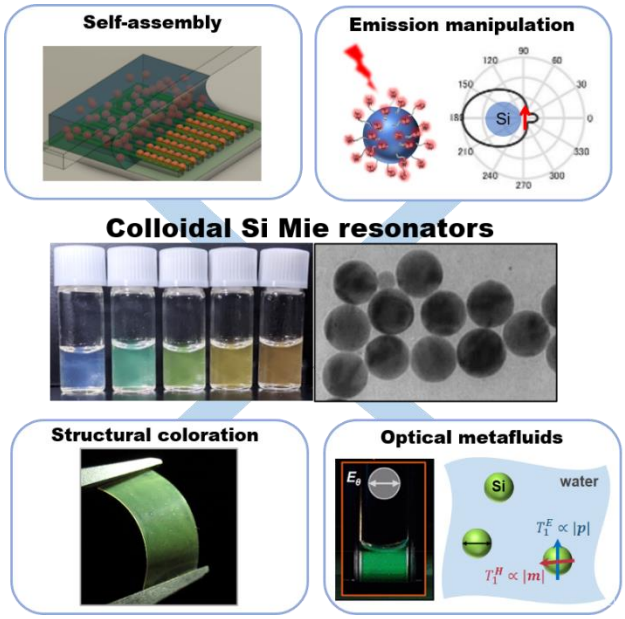

Figure 1. Colloidal Si nanoparticles and functionalities.

2. Preparation of colloidal dispersion of spherical Si particles

2.1 Amorphous Si particles

Almost perfectly spherical particles of hydrogenated amorphous Si (a-Si:H) have been produced in a few groups. In pioneering work by Korgel group in 2004, [35] they fabricated colloidal a-Si:H NPs 50 to 1500 nm in diameters (D_{Si}) by thermal decomposition of trisilane (Si_3H_8) at temperatures ranging from 400 to 500 °C. The average D_{Si} was controlled by the amount of Si_3H_8 in the reactor. Figure 2a-d shows SEM images of a-Si:H particles.[36] The particles are almost spherical. The standard deviation of the D_{Si} is less than 10% of the average D_{Si}.

Similarly, Fenollosa and Meseguer produced micron-size a-Si particles by using disilane (Si_2H_6) as a precursor.[37] The particles are crystallized by post annealing in vacuum at 800 ºC for 1 h. Figure 2e shows SEM images of polycrystalline Si microparticles. The D_{Si} is about 1-3 μm. The enlarged image in Fig. 2f shows the perfectly spherical shape and the smooth surface. The polycrystalline nature of the particles is confirmed by transmission electron microscope (TEM) observations; the crystalline domain size is about 10 nm.[38]

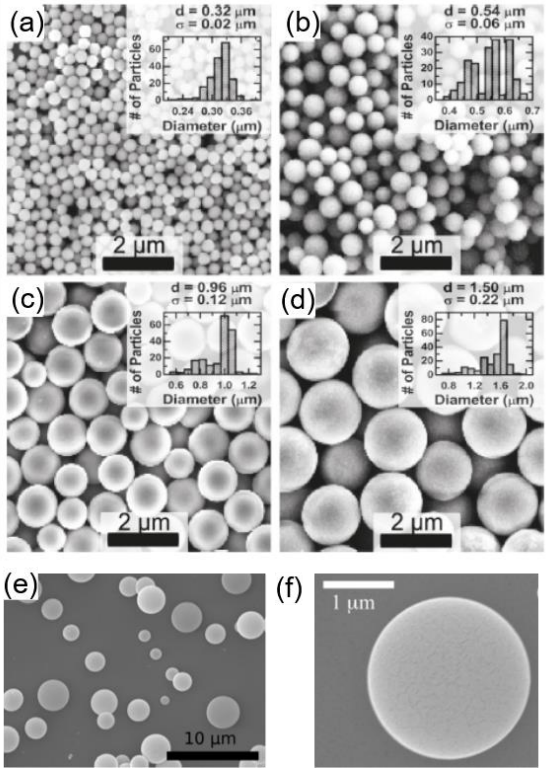

Figure 2. (a-d) SEM images of a-Si:H NPs. The amount of precursor (Si_3H_8) is increased from (a) to (d). Insets show particles size distributions. (e, f) SEM images of polycrystalline Si particles. (a-d) Reproduced with permission from [36]. Copyright 2010, American Chemical Society. (e, f)

Reproduced with permission from [39]. Copyright 2008, WILEY-VCH.

2.2 Crystalline Si nano- and micro-particles

As will be shown later, crystallinity is an important factor to achieve high-Q resonance in Si NPs. Our group developed a process to produce a colloid solution of spherical Si NPs with high crystallinity.[40] The fabrication process is based on high temperature thermal disproportionation of silicon monoxide (SiO) into Si and SiO_2. When the temperature is above the melting point of bulk Si crystal (1414 °C) and below that of silica (1710 °C), spherical crystalline Si (c-Si) NPs are grown in a SiO_2 matrix. The NPs are liberated from the matrix by hydrofluoric acid etching. Figure 3a shows a TEM image of c-Si NPs grown at 1500 °C. Almost perfectly spherical particles are grown. Lattice fringes in Figure 3b correspond to {111} planes of Si crystal. No thick oxide is formed on the surface. The average D_{Si} can be controlled by the annealing temperatures (Fig. 3c). Note that annealing at temperatures higher than the melting point of bulk Si crystal is a requisite condition to grow spherical NPs exhibiting the lowest order Mie resonance in the visible range, i.e., D_{Si} > ~100 nm. Figure 3d shows a Raman scattering spectrum of Si NPs grown at 1500 °C together with that of bulk Si crystal. The sharp transverse optical (TO) phonon peak at 520 cm^{-1} confirms the high crystallinity.

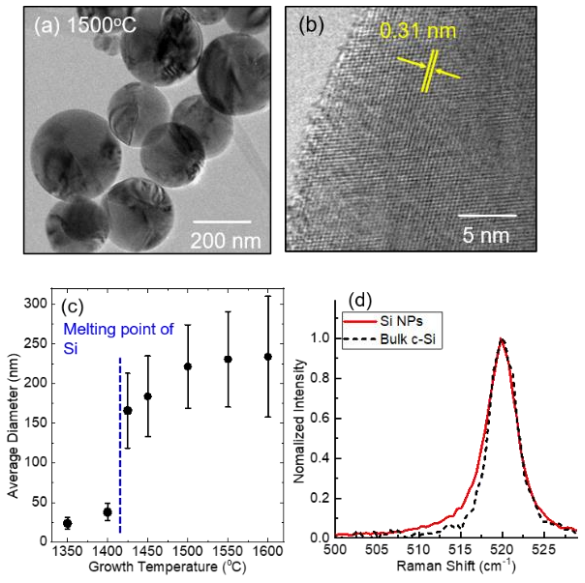

Figure 3. (a) TEM and (b) HRTEM images of c-Si NPs. (c) Average diameters of c-Si NPs grown at different temperatures. (d) Raman scattering spectra of c-Si NPs (solid red curve) and bulk Si crystal (black dashed curve). (a-d) Reproduced with permission from [40]. Copyright 2018, WILEY-VCH.

Another method to obtain spherical Si NPs is laser melting of irregular shape Si NPs in solution. Koshizaki and co-workers produced micro- and submicro-meter c-Si particles by irradiating water suspension of irregular shape Si particles by second harmonic of pulsed Nd:YAG laser (532 nm).[41,42] Figure 4a and b shows SEM images of starting materials, i.e., ball milled powder, and after laser melting, respectively. The shape is converted to be almost spherical. The size is around 1μm. The size can be reduced to 100 to 300 nm by reducing the size of starting particles and by using shorter wavelength for laser melting for larger absorption on the surface.[42] They demonstrated that using third harmonic of Nd:YAG laser (355 nm), the size is significantly reduced.[42] However, the sphericity is not as high as that of larger particles in Fig. 4b.

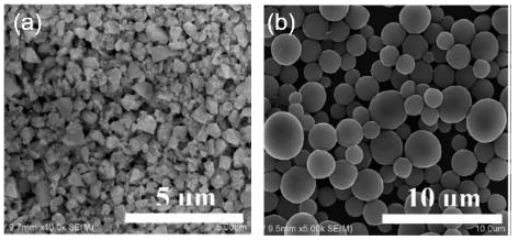

Figure 4. (a) SEM image of micron-sized c-Si particles prepared by ball milling. (b) SEM image after laser melting (irradiation by second harmonic of pulsed Nd:YAG laser (532 nm)). (a, b) Reproduced with permission from [41]. Copyright 2011, American Chemical Society.

3. Mie resonance of single Si particles

Prior to discussion on optical responses of colloidal solutions of Si NPs, we summarize scattering properties of individual Si particles on a substrate deposited from a colloidal dispersion. Following the size dependence of the scattering spectra, we refer to the importance of the crystallinity to achieve high Q resonance. We then present spectroscopic technique to measure angle- and polarization-resolved scattering spectra of a single Si NP. This allows us to detect ED and MD responses of a Si NP independently. We also show spectroscopic technique to selectively excite either electric or magnetic modes of a single Si NP. These techniques developed for the characterization of single particles are indispensable for the analyses of optical responses of Si NP assemblies produced from the colloidal solution.

3.1 Scattering spectra of single Si particles

We first discuss scattering spectra of single Si NPs drop-casted on a substrate and demonstrate that they exhibit Mie resonances predicted by the Mie theory. Figure 5a shows dark field (DF) scattering spectra and corresponding scattering images of different size (105-200 nm in diameter) single c-Si NPs placed on a glass substrate. Peaks corresponding to the lowest order magnetic (MD) and electric (ED) resonances are clearly observed. The peaks shift to longer wavelength and the scattering color changes from bluish to reddish with

increasing the size. The measured spectra agree well with those calculated by the Mie theory (gray dashed lines). A slight difference is due to the presence of the glass substrate,[43] which is not taken into account in the analytical Mie calculation.

Figure 5b shows scattering spectra of a measured and calculated c-Si NP 220-330 nm in diameters. The 2nd and 3rd order Mie modes, i. e., quadrupole (EQ and MQ) and octupole (EO and MO) modes appear in the visible range. The agreement between measured and calculated spectra are again fairly well. In general, higher order modes have higher Q-factor; the Q-factor of the EQ mode of a 330 nm c-Si NP at 715 nm is around 20, which is higher than those of the ED and MD modes in Figure 5a. Figure 5c shows the measured and calculated scattering spectra of a 2826±6 nm c-Si microparticle prepared by thermal annealing of an a-Si particle.[44,45] Higher-order Mie modes called whispering gallery modes (WGMs) are clearly observed. The Q-factor of the modes exceeds 1000. Overall the measured spectrum (black curve) agrees with the calculated (red curve) one.

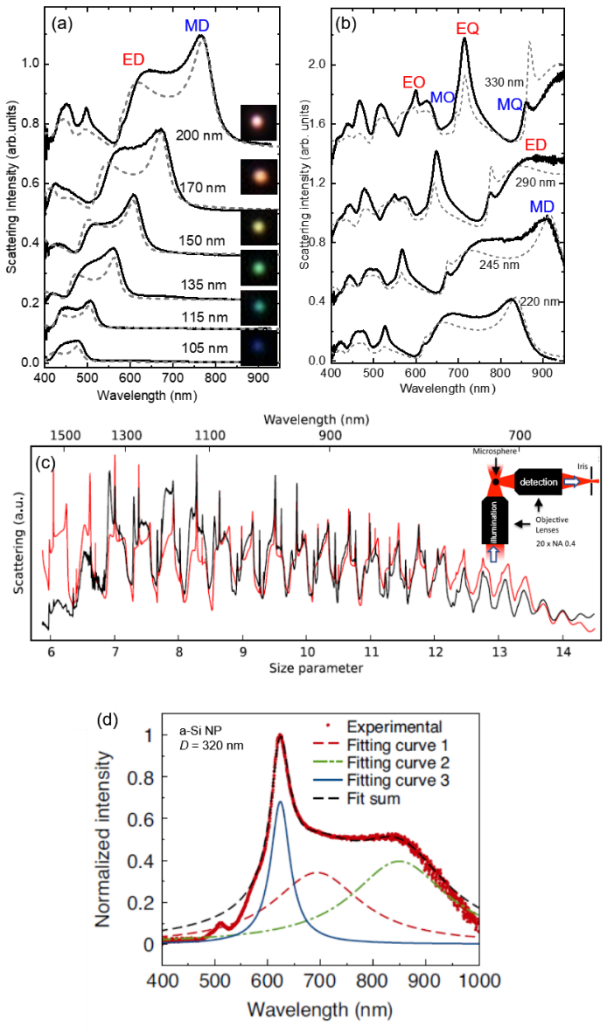

Figure 5. (a, b) Measured (black solid curve) and calculated (gray dashed curve) scattering spectra of single c-Si NPs (a) 105-200 nm and (b) 220-330 nm in diameters placed on a glass substrate. (c) Measured (black curve) and calculated (red curve) scattering spectra of a single polycrystalline Si particle. Measurement setup is shown in the inset. (d) Measured (red curve) scattering spectrum of single a-Si NP 320 nm in diameter. Fitthing curves corresponding to MD (1), ED (2) and MQ (3) modes are also shown. (a,b) Reproduced with permission from [40]. Copyright 2018, WILEY-VCH. (c) Reproduced with permission from [44]. Copyright 2016, American Physical Society. (d) Reproduced with permission from [46]. Copyright 2020, Nature Publishing Group.

The spectrum in Figure 5d is obtained for an a-Si:H NP (D_{Si} = 320 nm).[46] The refractive index and extinction coefficient of c-Si and a-Si:H are compared in Ref.[46]. Because of the direct band gap nature, the extinction coefficient of a-Si around 1.6-1.8 eV (690-775 nm) is much larger than that of c-Si. As a result, the scattering spectrum of an a-Si:H NP is significantly different from that of c-Si NPs (Figure 5a, b). Only a distinct peak of a MQ mode (*i.e.*, fitting curve 3) is observed in the visible range and the other modes are not clearly seen despite the high sphericity. Therefore, to take full advantage of a Si-based dielectric resonator, high crystallinity is crucial. Note that the loss of a-Si:H NPs is engineered partly by annealing and by controlling the hydrogen content; sharper resonance appears above 700 nm after the treatment.[46]

3.2 Angle- and polarization resolved Mie scattering of single Si particles

An important feature of a dielectric Mie resonator is the anisotropic far-field radiation pattern arising from the interference between the electric and magnetic modes. For example, interference between the ED and MD modes results in Kerker type forward and backward scattering of incident light [20,28,47]. Figure 6a and b shows the setups for the measurements of forward (FW) and backward (BW) scattering of a single Si NP, respectively. The upper panel of Fig. 6c shows the FW and BW scattering spectra of a Si NP paced on a thin (~8 nm) SiO_2 membrane. The blue curve represents the FW /BW intensity ratio. The TEM image of the same Si NP is shown in the inset. The lower panel shows the corresponding scattering spectra obtained by the finite-difference time-domain (FDTD) simulations under the same excitation and collection geometries. In both the FW and BW scattering geometries, the experimental and calculated spectra agree very well. The FW scattering is dominant around 650 nm, whereas BW scattering is dominant around 550 nm. These correspond to the 1st and 2nd Kerker conditions, respectively.

By slight modification of conventional DF optical microscope, it is possible to detect light scattered to almost arbitrary direction. Details of the setup can be found in Ref. [48]. By using the setup, we can separately detect the ED and

MD modes. For example, as schematically shown in the left panel of Figure 6d, when the incident light is p- (s-) polarized, scattered light to 90° direction with respect to the incidence is purely MD (ED) modes. Figure 6f and e shows measured and calculated scattering spectra of MD and ED modes, respectively. Measured and calculated spectra agree very well and thus the Mie modes of a single Si NP is separately detected by a conventional optical setup.

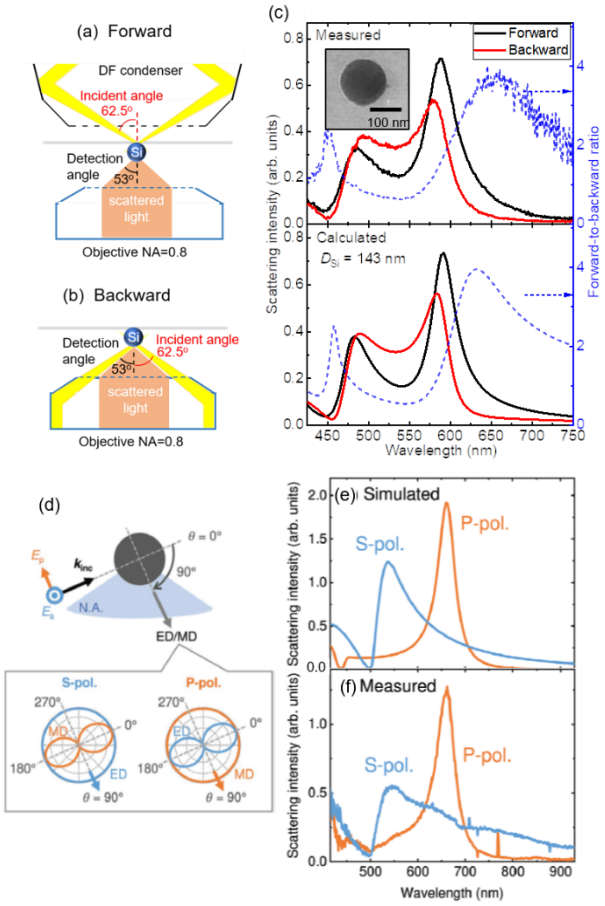

Figure 6. (a, b) Schematic illustration of the FW and BW scattering measurement setups. (c) Measured and calculated FW and BW scattering spectra of a Si NP (143 nm in diameter) shown in the inset. Blue dashed curves are the ratio of the FW/BW scattering spectra. (d) Schematic illustration of the geometry to selectively detect ED and MD Mie resonances. (e) Simulated and (f) measured scattering spectra under s- and p-polarized illumination. In the geometry in (e), ED and MD modes are selectively detected under s- and p- polarized illumination, respectively. (a-c) Reproduced with permission from [43]. Copyright 2019, WILEY-VCH. (d-f) Reproduced with permission from [48]. Copyright 2020, WILEY-VCH.

3.3 Mie scattering of single Si particles under structured illumination

In a highly symmetric spherical particle, illumination by conventional linearly and circularly polarized light result in excitation of both the electric and magnetic modes. On the other hand, specific modes can be selectively excited under structured illumination. This discloses other intriguing phenomenon regarding the Mie resonance of a spherical Si NP.[49–51] An example is the observation of the electromagnetic anapole state. The concept of anapole was first introduced in particle physics and recently has been of interest in nanophotonics community.[52–54] In the anapole state, interreference between a toroidal dipole (TD) mode, that is a current loop along a meridian of a torus in a dielectric resonator, and an electric dipole (ED) mode cancels the far field radiation (Figure 7a).[52] The ED and TD can be separately considered when the multipole expansion is done in Cartesian coordinate.[52] To excite the non-radiating anapole state, selective excitation of TD and ED modes without exciting other multipole modes are required. This condition is automatically fulfilled in a dielectric nanodisk (ND) with the diameter-to-height ratio higher than ~5. On the other hand, in a spherical Si NP, the MD mode interfere the anapole state. Manna et al.[50] demonstrated that a pure anapole state can be excited in a spherical c-Si NP by cylindrical vector beam illumination. As schematically shown in Fig. 7b, a focused radially polarized beam selectively excites the ED and TD modes with π phase difference. Figure 7c and d are measured and calculated scattering spectra, respectively, under linearly, radially and azimuthally polarized beam illumination. Under radially polarized illumination, the scattering intensity is closed to zero at 520 nm. From detailed theoretical analyses, the dip is assigned to the anapole state.[50]

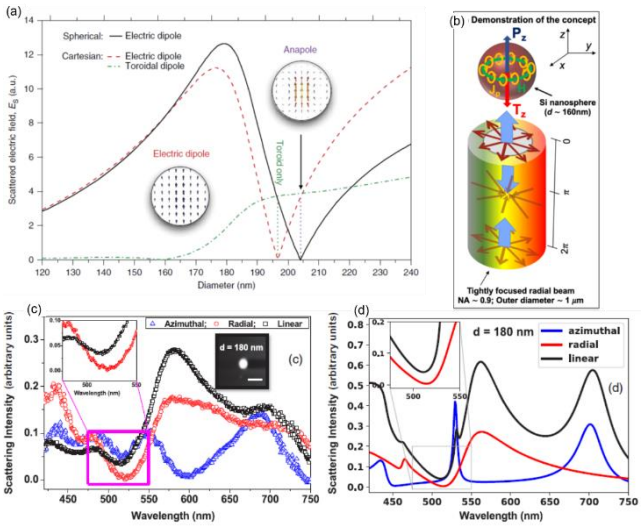

Figure 7. (a) Spherical ED and Cartesian ED and TD dipole moments contributions to scattering of a Si NP. (b) Schematic diagram showing illumination of a Si NP by radially polarized beam. (c) Measured and (d) simulated scattering spectra of

single Si NP under linear and vector beam (azimuthal and radial polarizations) illumination. (a) Reproduced with permission from [52]. Copyright 2015, Nature Publishing Group. (b-d) Reproduced with permission from [50]. Copyright 2020, American Physical Society.

3.4 Single Si particles placed on metal film

An advantage of colloidal Si NPs is that particles can be placed onto an arbitrary substrate by controlling the surface density. This allows us to study novel resonant modes arising from coupling of Mie resonances with a metallic substrate.[55–57] Figure 8a and b shows the dark-field scattering images of c-Si NPs on a silica substrate and on a Au film (200 nm in thickness), respectively.[58] On a silica substrate, green to yellow Mie scattering spots from 130-150 nm Si NPs are seen, while orange to red spots are seen on a Au film. The color change is due to the coupling, and the coupled structure is often called a Si NP on a Au mirror (SiNPoM) nanoantenna. Figure 8c compares scattering spectra of single SiNPoMs with different spacer thicknesses (1.2, 4.1, 7.0 and 12.8 nm). With decreasing the spacer thickness, a new mode emerges around 650 nm. This mode is a vertical ED mode of a Si NP coupled with its mirror-image in a Au film, and is responsible for the orange to red scattering color in Figure 8b.

A Si NP also acts as a nanoantenna to launch surface plasmon polaritons (SPPs) of a metal film. Recently, Assadillayev et al.[59] demonstrated coupling between Mie resonances of a Si NP and SPPs of a Au film using electron energy-loss spectroscopy (EELS) (Figure 8d). Figure 8e shows a EELS response of thin Au film (10 nm in thickness) caused by the excitation of the short range SPPs. The spectrum is very broad with the width of ~1 eV. By placing a Si NP on the Au film, the EELS spectrum becomes narrow and red-shifts (Fig. 8f). Detailed analyses revealed that these changes are due to the formation of a hybrid dielectric–plasmon resonance mode (electric field map in the inset of Fig. 8f) in the coupled system. [59]

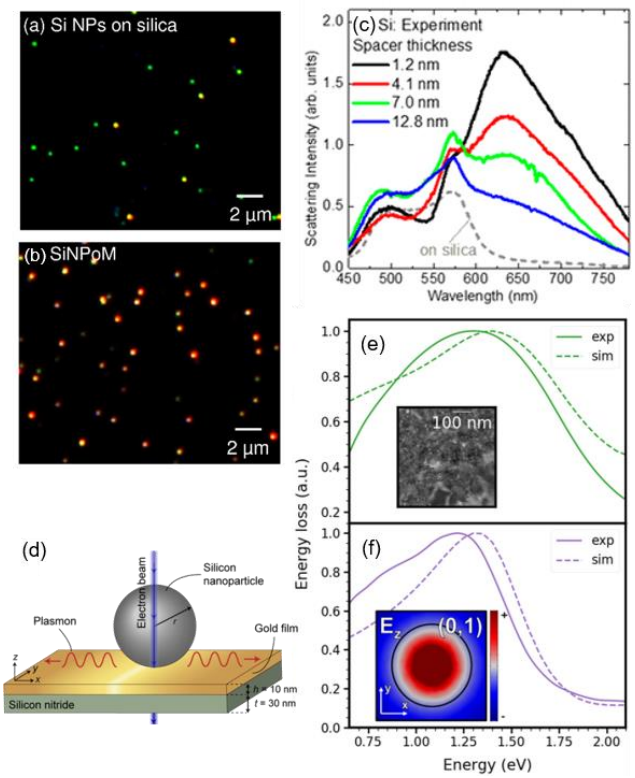

Figure 8. (a) Dark-field scattering images of (a) Si NPs on silica substrate and (b) Si NPs on Au mirror (SiNPoM). (c) Measured scattering spectra of single SiNPoMs with different spacer thicknesses of 1.2, 4.1, 7.0, and 12.8 nm. Spectrum of a NP on silica substrate is also shown (gray dashed curve). (d) Schematic of EELS measurement of a Si NP placed on a thin layer stack consisting of a 10 nm Au film on top of a 30 nm Si nitride membrane. (e, f) Measured and simulated EELS spectra of the structure without (e) and with (f) a Si NP. The radius of the particle is 54 nm. The inset in (f) shows the z-component of the electric field of the (0, 1) hybrid mode. (a-c) Reproduced with permission from [58]. Copyright 2018, American Chemical Society. (d-f) Reproduced with permission from [59]. Copyright 2021, American Chemical Society.

4. Enhancement of light matter interaction by single Si particles

Colloidal Si NPs can be placed on an arbitrary optical active material and can work as a nanoantenna to enhance the absorption, emission and Raman scattering, and to control the emission directionality. Furthermore, composite systems, in which optically active materials are directly attached on the surface of a Si NP, can be produced easily by a solution process. In this section, we present recent studies on the enhancement of absorption and fluorescence by Si NP nanoantennas.

4.1 Absorption Enhancement by Si NP antenna

Although the extinction coefficient of c-Si is small in the visible to near IR range, Mie resonance strongly confines an electric field in a Si NP and can effectively enhances the absorption cross section. Garín et al.[39] quantitatively discussed the absorption enhancement by a Si NP. They introduced a spectral averaged absorption enhancement ratio, $\xi = (\int_{\lambda_1}^{\lambda_2} \alpha_v(\lambda)E(\lambda)d\lambda)/(\int_{\lambda_1}^{\lambda_2} \alpha(\lambda)E(\lambda)d\lambda)$, as a figure of merit. In this equation, $E(\lambda)$ is the irradiance spectrum, α is the absorption coefficient of bulk c-Si and α_v is the volume absorption coefficient defined as $\alpha_v = q_a s/v$, where $s = \pi r^2$ and

$v = (4/3)\ \pi r^3$ are the cross section and volume of the particle, respectively, and q_a is the dimensionless absorption efficiency obtained by diving the absorption cross section by s. Figure 9a shows calculated ξ as a function of a particle diameter for different spectral ranges (λ_1=250, 450 and 750 nm, λ_2=1400 nm) considering the normalized sun spectrum AM1.5G. When the spectral range of incident light is 450-1400 nm, $\xi > 5$ in a 100-200 nm diameter Si NP. If the spectral range is limited to the NIR region (750-1400nm), the enhancement reaches 14 for a 200 nm particle. They suggest to utilize the enhanced absorption to a solar cell (Figure 9b). [39] The same group experimentally demonstrated absorption enhancement in a spherical Si microparticle in the IR range.[45]

Zograf et al.[60] monitored enhanced light absorption by a c-Si NP by Raman-based nanothermometry (Figure 9c). Figure 9d shows temperature rise (ΔT) as a function of D_{Si} under 633 nm light illumination. ΔT depends strongly on the D_{Si}, while that is almost independent of the size in a Au NP. A Si NP with a magnetic quadrupolar Mie resonance converts light to heat up to 4 times more effectively than similar Au NP at the same heating condition. [60] Later, Milichko et al.[61] demonstrated that controlled local optical heating up to 1200 K is possible in a metal-dielectric hybrid nanocavity composed of a Si NP and a Au film.

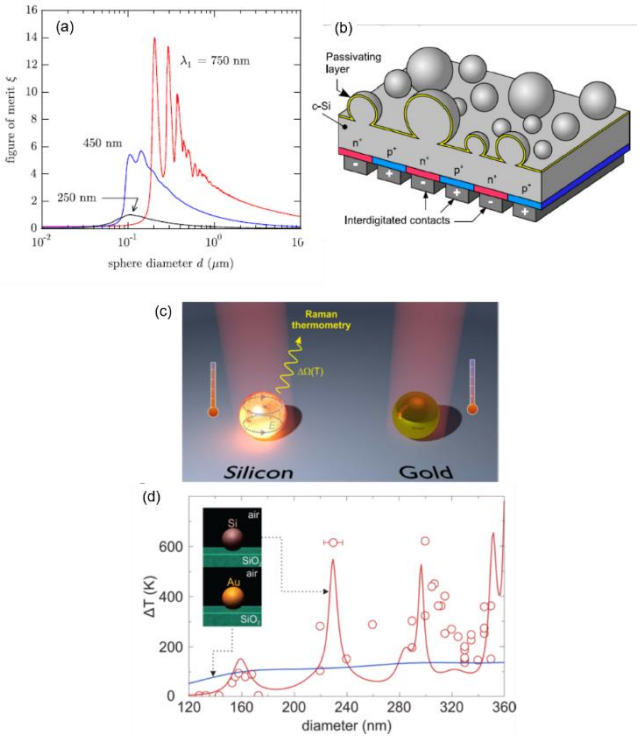

Figure 9.(a) Figure of merit for different wavelength bands $\lambda_1<\lambda<1400$nm (λ_1=250, 450 and 750 nm) as a function of Si NP diameter. (b) A solar cell incorporating Si micro- spheres working as both scatterers and absorbers. (c) Schematic illustration of optical heating of c-Si and Au NPs. The temperature of Si NPs can be measured by Raman thermometry. (d) Experimental (red circles) and numerically calculated (solid lines) temperature rise (ΔT) by light irradiation (λ = 633 nm, light intensity I_0 = 2 mW/μm^2) to Si (red) and Au (blue) NPs as a function of diameter. (a-b) Reproduced with permission from [39]. Copyright 2016, AIP Publishing LLC. (c-d) Reproduced with permission from [60]. Copyright 2017, American Chemical Society.

4.2 Emission enhancement by Si NP antenna

The enhanced electromagnetic field of a Si NP can be used to enhance light-matter interaction of nearby materials.[62–65] When an emitter is placed near a Si NP, the enhancement factor (EF) of the fluorescence intensity is expressed as,[2]

$$EF = \frac{\gamma_{ex}^{NP}}{\gamma_{ex}^{ref}} \frac{QE^{NP}}{QE^{ref}} \frac{\eta^{NP}}{\eta^{ref}}, \quad (1)$$

where γ_{ex} is the excitation rate of an emitter, QE is the quantum efficiency, and η is the emission collection efficiency. The superscripts "NP" and "ref" indicate the emitter with and without a Si NP, respectively. In the linear regime, γ_{ex} is proportional to the electric field intensity ($|E|^2$) at the emitter position. Figure 10a and b shows 2D maps of calculated extinction and averaged field intensity enhancement factors ($|E/E_0|^2$), respectively, of a c-Si NPs as functions of D_{Si} and the wavelength.[66] Averaging of the field intensity is made over the surface of a sphere 5 nm away from the NP surface. The two figures have similar features, meaning that the field is enhanced around the extinction peaks. The $|E/E_0|^2$ reaches 10 at the MQ resonance wavelength. Fluorescence enhancement via enhanced fields of a Si NP is demonstrated experimentally, [67] and summarized in review papers.[37,41]

A Si NP modifies the spontaneous emission rate of a nearby emitter via the Purcell effect.[68,69] Figure 10c shows the enhancement factor of the radiative rate ($\gamma_r^{NP}/\gamma_r^{ref}$) of a point dipole placed 5 nm from the Si NP surface as a function of wavelength. The data of dipoles with two different orientations are shown. A perpendicular dipole couples efficiently to the ED and EQ modes, while a parallel one couples to the MD and MQ modes.

In addition to the radiative rate enhancement, a new nonradiative decay process is introduced when an emitter is near a Si NP, which should be taken into account for the discussion of QE enhancement. Considering the new nonradiative decay process introduced by a Si NP, QE of an emitter near a Si NP QE^{NP} becomes

$$QE^{NP} = \frac{\gamma_r^{NP}/\gamma_r^{ref}}{(\gamma_r^{NP}+\gamma_{nr}^{NP})/\gamma_r^{ref}+(1-QE^{ref})/QE^{ref}}, \quad (2)$$

where γ_{nr}^{NP} is the nonradiative decay rate. If the intrinsic QE of an emitter is 1, QE^{NP} becomes $\gamma_r^{NP}/(\gamma_r^{NP}+\gamma_{nr}^{NP})$. This value is called an antenna efficiency. In a c-Si NP, the antenna efficiency is ~0.5 in the visible range, which is much higher than those of Ag and Au NPs, and QE enhancement is expected if the intrinsic QE of an emitter is smaller than the antenna efficiency. QE enhancement by a Si NP is experimentally demonstrated in a Si NP on a mirror structure, i.e., a Si NP is placed on a Au mirror via a monolayer of light

emitting quantum dots (QDs).[58]. A rough estimation suggests that *QE* enhancement reaches 700-fold compared to that of QDs on a Au mirror at the hot spot. Later, Yang et al. demonstrated 42-fold enhancement of the luminescence decay rate in a similar structure.[70]

Because of the anisotropic radiation pattern of a Si NP, the emission collection efficiency of a emitter (η^{NP}/η^{ref}) is strongly modified near a Si NP. Figure 10d and e shows radiation patterns of a dipole coupled perpendicular and parallel, respectively, to a Si NP. The wavelength is in between the ED and MD mode (670 nm). In the perpendicular coupling (Figure 10e), the radiation pattern is only slightly modified. On the other hand, in the parallel coupling, the dipole emits preferentially to the NP side. This is due to the Kerker effect under a dipole excitation.[71]

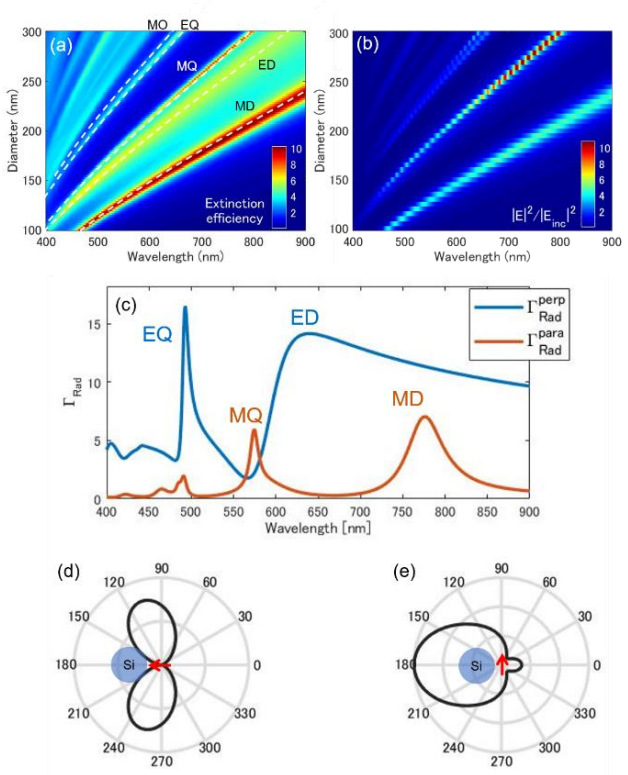

Figure 10. Contour plots of (a) extinction and (b) electric field intensity as a function of Si NP diameter and wavelength. (c) Radiative rate enhancement spectra of a dipole placed 5 nm from 200 nm-diameter c-Si NP surface. (d, e) Radiation patterns of perpendicular and parallel dipoles near Si NP. Red arrows indicate emitting dipoles.

Directional emission of a parallel dipole by a Si NP was recently experimentally confirmed by Cihan et al. for a monolayer transition metal dichalcogenide (TMDC) that has only parallel dipoles. [72] They placed a-Si NPs on a monolayer tungsten disulfide (WS_2) flake by drop-casting, and recorded the emission to the FW and BW directions. The FW/BW intensity ratio obtained for 125 NPs with different sizes show a clear size dependence and the trend agrees well with the theoretical prediction. The measured FW/BW intensity ratio is ~5 times smaller than the calculated one. This is mainly due to detection of emission from uncoupled WS_2 emitters around a Si NP in addition to that from coupled ones, i.e., those just beneath a Si NP. This problem can be avoided by removing undesired regions by a self-mask etching process.[71] Note that better directionality is expected if a c-Si NP instead of an a-Si NP is used because of the higher Kerker directionality due to the lower loss in the visible range.

4.3 Magnetic dipole emission enhancement in Si NP-emitter composite system

Many of researches on emission enhancement by nanoantennas focus on electric dipole transitions. In addition to electric dipole transitions, a Si NP can enhance magnetic dipole transitions of an emitter (*i.e.*, magnetic Purcell effect) because of the possession of magnetic multipole resonances.[73–79] Figure 11a shows calculated radiative rate enhancement factors of isotropic magnetic and electric dipoles coupled to a 208 nm Si NP. The radiative rate of an isotropic magnetic dipole is largely enhanced at MD (800 nm) and MQ (590 nm) resonances of a Si NP. The enhancement factors are much larger than those of an isotropic electric dipole. The large magnetic Purcell enhancement is not possible in metallic NPs due to the lack of magnetic multipole resonances.[80]

We recently succeeded in achieving large magnetic Purcell enhancement in a composite NP composed of a c-Si NP covered by a monolayer of Eu complexes ($Eu(DBM)_3phen$) (Figure 11b).[81] Figure 11c shows single particle scattering spectrum of a composite NP. The D_{Si} is 208 nm. The vertical broken lines represent the MQ resonance wavelength. Figure 11d shows the PL spectrum of the same NP. We can see that the magnetic dipole transition ($^5D_0$-$^7F_1$) of Eu^{3+} at 590 nm is strongly enhanced compared to the reference sample. The same experiments are performed for 16 single Si NPs and the results are summarized in Figure 11e. The ordinate of Figure 12e is the enhancement factor (G_{590}/G_{610}) of the PL intensity ratio ($G_{590} = I_{590}/I_{590\_ref}$ and $G_{610} = I_{610}/I_{610\_ref}$) of the magnetic dipole (I_{590}) and electric dipole (I_{610}) transitions of Eu^{3+}. The G_{590}/G_{610} has a clear peak at D_{Si}~208 nm. The enhancement factor reaches 11. This value is much higher than those reported for Si nanodisk arrays.[75] On the right axis of Figure 11e, calculated radiative rate enhancement factors (Γ_{rad}/Γ_0) of an isotropic magnetic dipole placed 5 nm from NP surface are shown. The radiative rate enhancement at D_{Si}~208 nm is due to the MQ resonance and that at D_{Si}~140 nm due to the MD resonance. Therefore, large enhancement of G_{590}/G_{610} at D_{Si}~208 nm is due to the MQ resonance.

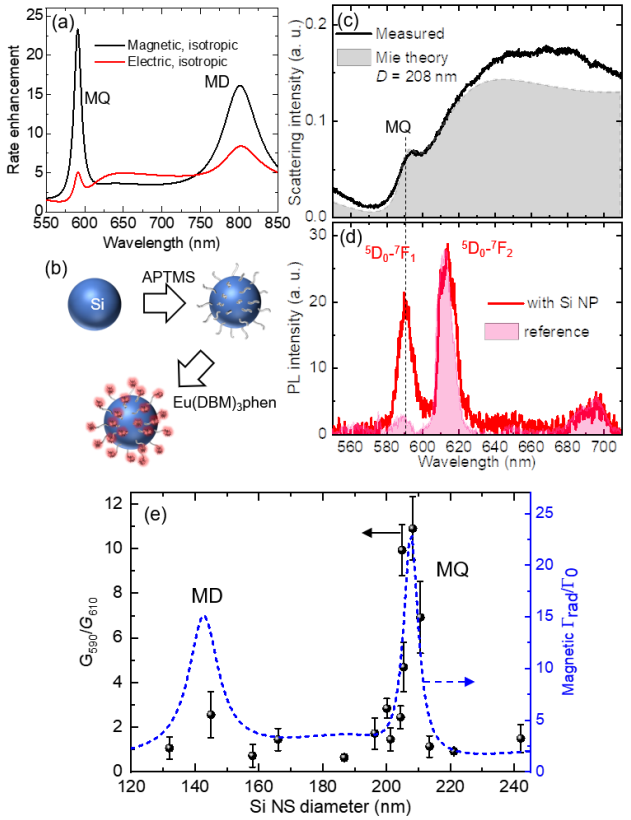

Figure 11. (a) Radiative rate enhancement factors for an isotropic magnetic dipole (black curve) and an isotropic electric dipole (red curve). (b) Schematic of preparation procedure of Si-NP: Eu(DBM)$_3$phen. (c) Scattering and (d) PL spectra of a single Si NP:Eu particle with D_{Si} = 208 nm. Gray and pink shaded spectra are calculated scattering and PL spectra of a reference sample, respectively. (e) The ratio of the enhancement factors of the 590 nm peak to the 610 nm peak (G_{590}/G_{610}) (black dots), and calculated radiative rate enhancement factor of an isotropic magnetic dipole moment placed 5 nm from NP surface (Γ_{rad}/Γ_0) (blue curve) as a function of D_{Si}. (a-e) Reproduced with permission from [81]. Copyright 2021, American Chemical Society.

5. Optical response of the colloidal solution

Finally, we discuss optical resonances of colloidal solutions, i.e., ensemble of a large number of Si NPs randomly distributed. Colloidal solutions of both c- and a-Si NPs have been produced.[29,30,82,83] In a-Si NPs, the optical response has been studied in the near-IR range for solutions of monodispersed NPs with a relatively larger size (D_{Si} > 380 nm).[30] However, there have been no systematic studies in the visible range due to the large absorption loss as discussed in Section 3.1. In c-Si NPs, the large size distribution [29] and the small scale production of size-purified NPs [82] had been the obstacles for the observation of Mie resonance-derived optical phenomena in a macroscopic scale. In this section, we introduce recent advancements in the production of colloidal c-Si NPs exhibiting clear Mie resonances in macroscopic measurements. Macroscopic observation of Mie resonance-derived phenomena leads to application of the colloidal solutions in structural coloration and as optical metafluids.

Mie resonant Si NPs with 100-200 nm in diameter efficiently scatter incoming light at the resonance wavelength and exhibit scattering-induced reflection colors as shown in Figure 5a. Therefore, high-resolution coloring is possible using Si nanostructures. This has been demonstrated for a planar Si nanostructures produced by electron beam lithography.[84–88] Although structural coloring by Si nanostructures is a very attractive, the size of the coloration area produced by conventional nanofabrication technology is very small and thus the practical usage is limited. The low throughput is also the case for laser printing methods.[89,90] To realize large area structural coloration by Si nanostructures, inks of c-Si NPs that are capable of being coated or inkjet printed on a substrate should be developed.[40] Since Mie resonance wavelengths depend on Si NP size, reduction of the size distribution is crucial to exploit vivid scattering color of individual Si NPs in macroscopic scale NP inks. Figure 13a shows a TEM image of Si NPs in a colloidal solution size-purified by a density-gradient centrifugation. The size distribution is less than 10% of the average D_{Si}. The solutions of different average D_{Si} exhibit vivid colors (Figure 12b). The reflectance spectra of the solutions are converted to color space in Fig. 12c. By changing the Si NP size from 95 to 200 nm, a wide area of sRGB is covered. Inks of Si NP solution and polymer binder can paint a macroscopic size flexible substrate (Figure 12d).

Since coloration of Si NP inks is mainly due to scattering not due to absorption, the color depends on the concentration and the optical path length. In order to predict the reflection color precisely of a solution, we develop a Monte-Carlo simulation code by taking into account Mie scattering of individual NPs. Furthermore, we extend the code to treat a mixture ink of Si NPs and light-absorbing carbon black (CB) NPs.[91] We experimentally demonstrate that the combination of Kerker-type back scattering of a Si NP and a broad absorption by a CB NP allows us to control the hue, saturation and brightness of an ink in a wide range and to realize vivid reflection colors under room light (Figure 12e).

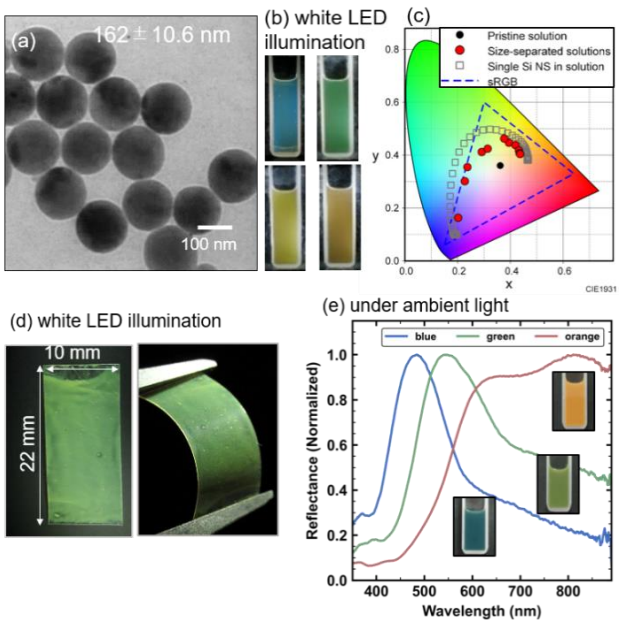

Figure 12. (a) Typical TEM image of spherical Si NPs in size-separated solution. (b) Photographs of solutions of size-separated Si NPs. (c) CIE1931 chromaticity diagram and color space values obtained from diffuse reflectance spectra. (d) Photograph of Si NPs-polyvinylpyrrolidone (PVP) film on polyethylene terephthalate (PET) substrate. (e) Normalized reflectance spectra and photos of Si NP-CB NP mixture inks. (a-d) Reproduced with permission from [40]. Copyright 2018, WILEY-VCH. (e) Reproduced with permission from [91]. Copyright 2021, American Chemical Society.

Our achievement to produce inks of almost monodispersed Si NPs opens a new horizon toward the development of liquids with optical magnetism and those with unnaturally high or low effective refractive indices. These liquids are called optical metafluids and first developed using plasmonic nanoparticle clusters[92,93] Recently, Hinamoto et al.[94] demonstrated that a colloidal dispersion of size-purified c-Si NPs exhibits a strong magnetic response in the visible range. Because of the difference in the scattering pattern and the polarization of the ED (*p*, blue) and MD (*m*, orange) modes as shown in Figure 13a, each dipolar response is separately measured by the setup in Fig. 13b. Figure 13c shows photographs and measured and calculated scattering spectra of metafluids containing different size Si NPs. MD and ED responses are separately measured and it can be recognized as the scattering color difference. The MD/ED intensity ratio is almost unity, which is higher than those reported for plasmonic metafluids in the visible range.

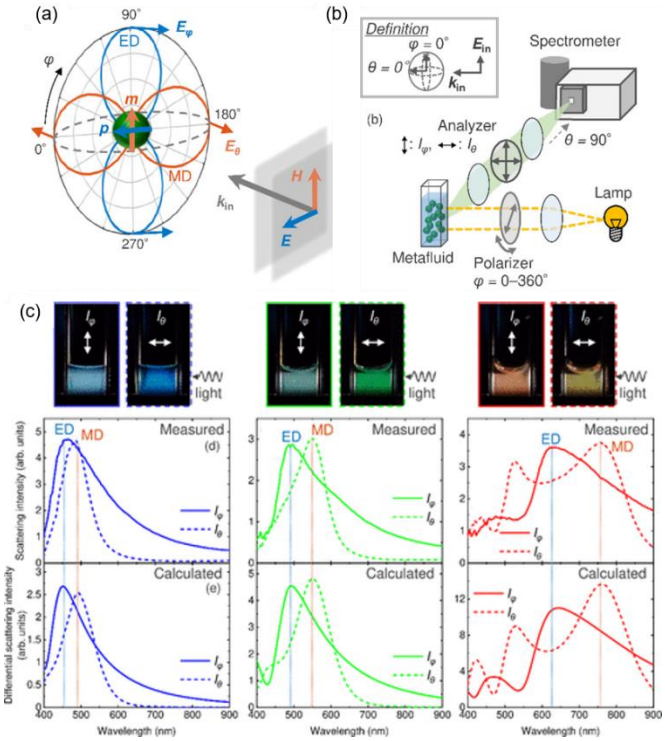

Figure 13. Radiation patterns of ED and MD moments-resolved scattering spectroscopy. (a) Scattering patterns and orientations of electric fields of ED (p, blue) and MD (m, orange) moments. (b) Setup for the angle- and polarization-resolved scattering measurements. (c) Photographs and measured and calculated scattering spectra of the blue, green, and red metafluids in the I_φ (φ=90°) and I_θ (φ=0°) configurations in (b). (a-c) Reproduced with permission from [94]. Copyright 2021, American Chemical Society.

Summary and Outlook

In the first half of this review, we have presented recent development of the synthesis of colloidal c-Si NPs. We showed that the quality of the state-of-the-art c-Si NPs is very high and that the light scattering properties, including angle- and polarization dependent scattering properties, are almost identical to those predicted by the Mie theory of spherical Si NPs. These high-quality Si NPs act as nanoantennas for the enhancement of absorption and emission of nearby materials. In particular, they exhibit the strong magnetic Purcell effect that is not possible in spherical plasmonic NPs. The improvement of the quality of colloidal Si NPs, including the drastic narrowing of the size distribution, makes the microscopic Mie resonant properties to appear in macroscopic solutions containing huge number of Si NPs. Typical examples are structural coloration by Si NP inks and Si NP metafluids having large optical magnetism. We believe that the research on colloidal Si NPs is moving to the next stage. We are now ready to embark on programmed assembly of Si

NPs by a solution-based process to achieve new functionality for sensing and imaging applications.

Acknowledgements

H. S. acknowledge the supported by JST, PRESTO Grant Number JPMJPR19T4, Japan. This work is partly supported also by JSPS KAKENHI Grant Numbers 18KK0141 and 21K14496.

References

[1] Giannini V, Fernández-Domínguez A I, Heck S C and Maier S a. 2011 Plasmonic nanoantennas: Fundamentals and their use in controlling the radiative properties of nanoemitters *Chem. Rev.* **111** 3888–912

[2] Novotny L and Hecht B 2006 *Principles of Nano-Optics* (Cambridge: Cambridge University Press)

[3] Campion A and Kambhampati P 1998 Surface-enhanced Raman scattering *Chem. Soc. Rev.* **27** 241

[4] Smith W E 2008 Practical understanding and use of surface enhanced Raman scattering/surface enhanced resonance Raman scattering in chemical and biological analysis. *Chem. Soc. Rev.* **37** 955–64

[5] Akselrod G M, Argyropoulos C, Hoang T B, Ciracì C, Fang C, Huang J, Smith D R and Mikkelsen M H 2014 Probing the mechanisms of large Purcell enhancement in plasmonic nanoantennas *Nat. Photonics* **8** 835–40

[6] Dong J, Zhang Z, Zheng H and Sun M 2015 Recent Progress on Plasmon-Enhanced Fluorescence *Nanophotonics* **4** 472–90

[7] Boardman A D and Zayats A V. 2014 Nonlinear plasmonics *Handb. Surf. Sci.* **4** 329–47

[8] Walsh G F and Dal Negro L 2013 Enhanced Second Harmonic Generation by Photonic–Plasmonic Fano-Type Coupling in Nanoplasmonic Arrays *Nano Lett.* **13** 3111–7

[9] Fröhlich H 1949 Theory of dielectrics

[10] Brongersma M L, Halas N J and Nordlander P 2015 Plasmon-induced hot carrier science and technology *Nat. Nanotechnol.* **10** 25–34

[11] Kristensen A, Yang J K W, Bozhevolnyi S I, Link S, Nordlander P, Halas N J and Mortensen N A 2017 Plasmonic colour generation *Nat. Rev. Mater.* **2** 16088

[12] Ayala-Orozco C, Liu J G, Knight M W, Wang Y, Day J K, Nordlander P and Halas N J 2014 Fluorescence enhancement of molecules inside a gold nanomatryoshka *Nano Lett.* **14** 2926–33

[13] Chikkaraddy R, de Nijs B, Benz F, Barrow S J, Scherman O A, Rosta E, Demetriadou A, Fox P, Hess O and Baumberg J J 2016 Single-molecule strong coupling at room temperature in plasmonic nanocavities *Nature* **535** 127–30

[14] Bardhan R, Lal S, Joshi A and Halas N J 2011 Theranostic Nanoshells: From Probe Design to Imaging and Treatment of Cancer *Acc. Chem. Res.* **44** 936–46

[15] Aslan K, Gryczynski I, Malicka J, Matveeva E, Lakowicz J R and Geddes C D 2005 Metal-enhanced fluorescence: An emerging tool in biotechnology *Curr. Opin. Biotechnol.* **16** 55–62

[16] Kuznetsov A I, Miroshnichenko A E, Fu Y H, Zhang J and Luk'yanchuk B 2012 Magnetic light *Sci. Rep.* **2** 492

[17] Evlyukhin A B, Novikov S M, Zywietz U, Eriksen R L, Reinhardt C, Bozhevolnyi S I and Chichkov B N 2012 Demonstration of magnetic dipole resonances of dielectric nanospheres in the visible region *Nano Lett.* **12** 3749–55

[18] Kuznetsov A I, Miroshnichenko A E, Brongersma M L, Kivshar Y S and Luk'yanchuk B 2016 Optically resonant dielectric nanostructures *Science (80-.).* **354** aag2472

[19] Baranov D G, Zuev D A, Lepeshov S I, Kotov O V., Krasnok A E, Evlyukhin A B and Chichkov B N 2017 All-dielectric nanophotonics: the quest for better materials and fabrication techniques *Optica* **4** 814

[20] Liu W and Kivshar Y S 2018 Generalized Kerker effects in nanophotonics and meta-optics [Invited] *Opt. Express* **26** 13085

[21] Decker M, Staude I, Falkner M, Dominguez J, Neshev D N, Brener I, Pertsch T and Kivshar Y S 2015 High-Efficiency Dielectric Huygens' Surfaces *Adv. Opt. Mater.* **3** 813–20

[22] Paniagua-Domínguez R, Yu Y F, Khaidarov E, Choi S, Leong V, Bakker R M, Liang X, Fu Y H, Valuckas V, Krivitsky L A and Kuznetsov A I 2018 A Metalens with a Near-Unity Numerical Aperture *Nano Lett.* **18** 2124–32

[23] Cui C, Zhou C, Yuan S, Qiu X, Zhu L, Wang Y, Li Y, Song J, Huang Q, Wang Y, Zeng C and Xia J 2018 Multiple Fano Resonances in Symmetry-Breaking Silicon Metasurface for Manipulating Light Emission *ACS Photonics* **5** 4074–80

[24] Liu Z, Xu Y, Lin Y, Xiang J, Feng T, Cao Q, Li J, Lan S and Liu J 2019 High- <math display="inline"> <mi>Q</mi> </math> Quasibound States in the Continuum for Nonlinear Metasurfaces *Phys. Rev. Lett.* **123** 253901

[25] Leitis A, Tittl A, Liu M, Lee B H, Gu M B, Kivshar Y S and Altug H 2019 Angle-multiplexed all-dielectric metasurfaces for broadband molecular fingerprint retrieval *Sci. Adv.* **5** eaaw2871

[26] Jeong P A, Goldflam M D, Campione S, Briscoe J L, Vabishchevich P P, Nogan J, Sinclair M B, Luk T S and Brener I 2020 High Quality Factor Toroidal Resonances in Dielectric Metasurfaces *ACS Photonics* **7** 1699–707

[27] De Marco M L, Semlali S, Korgel B A, Barois P, Drisko G L and Aymonier C 2018 Silicon-Based

Dielectric Metamaterials: Focus on the Current Synthetic Challenges *Angew. Chemie Int. Ed.* **57** 4478–98

[28] Fu Y H, Kuznetsov A I, Miroshnichenko A E, Yu Y F and Luk'yanchuk B 2013 Directional visible light scattering by silicon nanoparticles *Nat. Commun.* **4** 1527

[29] Chaâbani W, Proust J, Movsesyan A, Béal J, Baudrion A-L, Adam P-M, Chehaidar A and Plain J 2019 Large-Scale and Low-Cost Fabrication of Silicon Mie Resonators *ACS Nano* **13** 4199–208

[30] Shi L, Harris J T, Fenollosa R, Rodriguez I, Lu X, Korgel B A and Meseguer F 2013 Monodisperse silicon nanocavities and photonic crystals with magnetic response in the optical region *Nat. Commun.* **4** 1904

[31] Hanske C, Tebbe M, Kuttner C, Bieber V, Tsukruk V V., Chanana M, König T A F and Fery A 2014 Strongly Coupled Plasmonic Modes on Macroscopic Areas via Template-Assisted Colloidal Self-Assembly *Nano Lett.* **14** 6863–71

[32] Chen T and Reinhard B M 2016 Assembling Color on the Nanoscale: Multichromatic Switchable Pixels from Plasmonic Atoms and Molecules *Adv. Mater.*

[33] Probst P T, Mayer M, Gupta V, Steiner A M, Zhou Z, Auernhammer G K, König T A F and Fery A 2021 Mechano-tunable chiral metasurfaces via colloidal assembly *Nat. Mater.*

[34] Mayer M, Schnepf M J, König T A F and Fery A 2019 Colloidal Self-Assembly Concepts for Plasmonic Metasurfaces *Adv. Opt. Mater.* **7** 1800564

[35] Pell L E, Schricker A D, Mikulec F V. and Korgel B A 2004 Synthesis of Amorphous Silicon Colloids by Trisilane Thermolysis in High Temperature Supercritical Solvents *Langmuir* **20** 6546–8

[36] Harris J T, Hueso J L and Korgel B A 2010 Hydrogenated amorphous silicon (a-Si:H) colloids *Chem. Mater.* **22** 6378–83

[37] Fenollosa R, Meseguer F and Tymczenko M 2008 Silicon Colloids: From Microcavities to Photonic Sponges *Adv. Mater.* **20** 95–8

[38] Meseguer F, Fenollosa R, Rodriguez I, Xifré-Pérez E, Ramiro-Manzano F, Garín M and Tymczenko M 2011 Silicon colloids: A new enabling nanomaterial *J. Appl. Phys.* **109** 102424

[39] Garín M, Fenollosa R, Ortega P and Meseguer F 2016 Light harvesting by a spherical silicon microcavity *J. Appl. Phys.* **119** 033101

[40] Sugimoto H, Okazaki T and Fujii M 2020 Mie Resonator Color Inks of Monodispersed and Perfectly Spherical Crystalline Silicon Nanoparticles *Adv. Opt. Mater.* **8** 2000033

[41] Li X, Pyatenko A, Shimizu Y, Wang H, Koga K and Koshizaki N 2011 Fabrication of Crystalline Silicon Spheres by Selective Laser Heating in Liquid Medium *Langmuir* **27** 5076–80

[42] Wakatsuki Y, Ishikawa Y and Koshizaki N 2020 Hydrofluoric acid pretreatment effect on the formation of silicon submicrometer particles by pulsed laser melting in liquid and their optical scattering property *Nanotechnology* **31** 095601

[43] Sugimoto H, Hinamoto T and Fujii M 2019 Forward to Backward Scattering Ratio of Dielectric–Metal Heterodimer Suspended in Almost Free-Space *Adv. Opt. Mater.* **7** 1900591

[44] Fenollosa R, Garín M and Meseguer F 2016 Spherical silicon photonic microcavities: From amorphous to polycrystalline *Phys. Rev. B* **93** 235307

[45] Garín M, Fenollosa R, Alcubilla R, Shi L, Marsal L F and Meseguer F 2014 All-silicon spherical-Mie-resonator photodiode with spectral response in the infrared region *Nat. Commun.* **5** 3440

[46] Wang M, Krasnok A, Lepeshov S, Hu G, Jiang T, Fang J, Korgel B A, Alù A and Zheng Y 2020 Suppressing material loss in the visible and near-infrared range for functional nanophotonics using bandgap engineering *Nat. Commun.* **11** 5055

[47] Kerker M, Wang D-S and Giles C L 1983 Electromagnetic scattering by magnetic spheres *J. Opt. Soc. Am.* **73** 765

[48] Hinamoto T, Hamada M, Sugimoto H and Fujii M 2021 Angle-, Polarization-, and Wavelength-Resolved Light Scattering of Single Mie Resonators Using Fourier-Plane Spectroscopy *Adv. Opt. Mater.* **9** 2002192

[49] Manna U, Sugimoto H, Eggena D, Coe B, Wang R, Biswas M and Fujii M 2020 Selective excitation and enhancement of multipolar resonances in dielectric nanospheres using cylindrical vector beams *J. Appl. Phys.*

[50] Parker J A, Sugimoto H, Coe B, Eggena D, Fujii M, Scherer N F, Gray S K and Manna U 2020 Excitation of Nonradiating Anapoles in Dielectric Nanospheres *Phys. Rev. Lett.* **124** 097402

[51] Manna U, Lee J-H, Deng T-S, Parker J, Shepherd N, Weizmann Y and Scherer N F 2017 Selective Induction of Optical Magnetism *Nano Lett.* **17** 7196–206

[52] Miroshnichenko A E, Evlyukhin A B, Yu Y F, Bakker R M, Chipouline A, Kuznetsov A I, Luk'yanchuk B, Chichkov B N and Kivshar Y S 2015 Nonradiating anapole modes in dielectric nanoparticles *Nat. Commun.* **6** 8069

[53] Baryshnikova K, Smirnova D, Luk'yanchuk B and Kivshar Y 2018 Optical anapoles in nanophotonics and meta-optics 1–14

[54] Wei L, Xi Z, Bhattacharya N and Urbach H P 2016 Excitation of the radiationless anapole mode *Optica* **3** 799

[55] Sinev I, Iorsh I, Bogdanov A, Permyakov D, Komissarenko F, Mukhin I, Samusev A, Valuckas V, Kuznetsov A I, Luk'yanchuk B S, Miroshnichenko A E and Kivshar Y S 2016 Polarization control over electric and magnetic dipole resonances of dielectric

nanoparticles on metallic films *Laser Photon. Rev.* **10** 799–806
[56] Li H, Xu Y, Xiang J, Li X F, Zhang C Y, Tie S L and Lan S 2016 Exploiting the interaction between a semiconductor nanosphere and a thin metal film for nanoscale plasmonic devices *Nanoscale* **8** 18963–71
[57] Xifré-Pérez E, Shi L, Tuzer U, Fenollosa R, Ramiro-Manzano F, Quidant R and Meseguer F 2013 Mirror-Image-Induced Magnetic Modes *ACS Nano* **7** 664–8
[58] Sugimoto H and Fujii M 2018 Broadband Dielectric-Metal Hybrid Nanoantenna: Silicon Nanoparticle on a Mirror *ACS Photonics* **5** 1986–93
[59] Assadillayev A, Hinamoto T, Fujii M, Sugimoto H, Brongersma M L and Raza S 2021 Plasmon Launching and Scattering by Silicon Nanoparticles *ACS Photonics* **8** 1582–91
[60] Zograf G P, Petrov M I, Zuev D A, Dmitriev P A, Milichko V A, Makarov S V. and Belov P A 2017 Resonant Nonplasmonic Nanoparticles for Efficient Temperature-Feedback Optical Heating *Nano Lett.* **17** 2945–52
[61] Milichko V A, Zuev D A, Baranov D G, Zograf G P, Volodina K, Krasilin A A, Mukhin I S, Dmitriev P A, Vinogradov V V., Makarov S V. and Belov P A 2018 Metal-Dielectric Nanocavity for Real-Time Tracing Molecular Events with Temperature Feedback *Laser Photon. Rev.* **12** 1700227
[62] Caldarola M, Albella P, Cortés E, Rahmani M, Roschuk T, Grinblat G, Oulton R F, Bragas A V and Maier S A 2015 Non-plasmonic nanoantennas for surface enhanced spectroscopies with ultra-low heat conversion. *Nat. Commun.* **6** 7915
[63] Krasnok A, Caldarola M, Bonod N and Alú A 2018 Spectroscopy and Biosensing with Optically Resonant Dielectric Nanostructures *Adv. Opt. Mater.* **6** 1701094
[64] Bidault S, Mivelle M and Bonod N 2019 Dielectric nanoantennas to manipulate solid-state light emission *J. Appl. Phys.* **126**
[65] Regmi R, Berthelot J, Winkler P M, Mivelle M, Proust J, Bedu F, Ozerov I, Begou T, Lumeau J, Rigneault H, García-Parajó M F, Bidault S, Wenger J and Bonod N 2016 All-Dielectric Silicon Nanogap Antennas to Enhance the Fluorescence of Single Molecules *Nano Lett.* **16** 5143–51
[66] Le Ru E C and Etchegoin P G 2009 *Principles of surface-enhanced Raman spectroscopy : and related plasmonic effects* (Amsterdam ; Boston : Elsevier)
[67] Sugimoto H and Fujii M 2017 Colloidal Dispersion of Subquarter Micrometer Silicon Spheres for Low-Loss Antenna in Visible Regime *Adv. Opt. Mater.* **5** 1700332
[68] Purcell E M 1995 Spontaneous Emission Probabilities at Radio Frequencies *Phys. Rev.* vol 69 pp 839–839
[69] Zambrana-Puyalto X and Bonod N 2015 Purcell factor of spherical Mie resonators *Phys. Rev. B* **91** 195422
[70] Yang G, Niu Y, Wei H, Bai B and Sun H-B 2019 Greatly amplified spontaneous emission of colloidal quantum dots mediated by a dielectric-plasmonic hybrid nanoantenna *Nanophotonics* **8** 2313–9
[71] Cihan A F, Curto A G, Raza S, Kik P G and Brongersma M L 2018 Silicon Mie resonators for highly directional light emission from monolayer MoS2 *Nat. Photonics* **12** 284–90
[72] Fang J, Wang M, Yao K, Zhang T, Krasnok A, Jiang T, Choi J, Kahn E, Korgel B A, Terrones M, Li X, Alù A and Zheng Y 2021 Directional Modulation of Exciton Emission Using Single Dielectric Nanospheres *Adv. Mater.* **33** 2007236
[73] Rolly B, Bebey B, Bidault S, Stout B and Bonod N 2012 Promoting magnetic dipolar transition in trivalent lanthanide ions with lossless Mie resonances *Phys. Rev. B - Condens. Matter Mater. Phys.* **85** 2–7
[74] Baranov D G, Savelev R S, Li S V., Krasnok A E and Alù A 2017 Modifying magnetic dipole spontaneous emission with nanophotonic structures *Laser Photon. Rev.* **11** 1600268
[75] Vaskin A, Mashhadi S, Steinert M, Chong K E, Keene D, Nanz S, Abass A, Rusak E, Choi D-Y, Fernandez-Corbaton I, Pertsch T, Rockstuhl C, Noginov M A, Kivshar Y S, Neshev D N, Noginova N and Staude I 2019 Manipulation of Magnetic Dipole Emission from Eu 3+ with Mie-Resonant Dielectric Metasurfaces *Nano Lett.* **19** 1015–22
[76] Li J, Verellen N and Van Dorpe P 2017 Enhancing Magnetic Dipole Emission by a Nano-Doughnut-Shaped Silicon Disk *ACS Photonics* **4** 1893–8
[77] Wiecha P R, Majorel C, Girard C, Arbouet A, Masenelli B, Boisron O, Lecestre A, Larrieu G, Paillard V and Cuche A 2019 Enhancement of electric and magnetic dipole transition of rare-earth-doped thin films tailored by high-index dielectric nanostructures *Appl. Opt.* **58** 1682
[78] Feng T, Xu Y, Liang Z and Zhang W 2016 All-dielectric hollow nanodisk for tailoring magnetic dipole emission *Opt. Lett.* **41** 5011
[79] Feng T, Zhang W, Liang Z, Xu Y and Miroshnichenko A E 2018 Isotropic Magnetic Purcell Effect *ACS Photonics* **5** 678–83
[80] Kruk S and Kivshar Y 2017 Functional Meta-Optics and Nanophotonics Governed by Mie Resonances *ACS Photonics* **4** 2638–49
[81] Sugimoto H and Fujii M 2021 Magnetic Purcell Enhancement by Magnetic Quadrupole Resonance of Dielectric Nanosphere Antenna *ACS Photonics* **8** 1794–800
[82] Valuckas V, Paniagua-Domínguez R, Maimaiti A, Patra P P, Wong S K, Verre R, Käll M and Kuznetsov A I 2019 Fabrication of Monodisperse Colloids of Resonant Spherical Silicon Nanoparticles: Applications in Optical Trapping and Printing *ACS Photonics* **6** 2141–8

[83] Verre R, Shao L, Odebo Länk N, Karpinski P, Yankovich A B, Antosiewicz T J, Olsson E and Käll M 2017 Metasurfaces and Colloidal Suspensions Composed of 3D Chiral Si Nanoresonators *Adv. Mater.* **29** 1701352

[84] Proust J, Bedu F, Gallas B, Ozerov I and Bonod N 2016 All-Dielectric Colored Metasurfaces with Silicon Mie Resonators *ACS Nano* **10** 7761–7

[85] Nagasaki Y, Suzuki M and Takahara J 2017 All-Dielectric Dual-Color Pixel with Subwavelength Resolution *Nano Lett.* **17** 7500–6

[86] Dong Z, Ho J, Yu Y F, Fu Y H, Paniagua-Dominguez R, Wang S, Kuznetsov A I and Yang J K W 2017 Printing Beyond sRGB Color Gamut by Mimicking Silicon Nanostructures in Free-Space *Nano Lett.* **17** 7620–8

[87] Vashistha V, Vaidya G, Hegde R S, Serebryannikov A E, Bonod N and Krawczyk M 2017 All-Dielectric Metasurfaces Based on Cross-Shaped Resonators for Color Pixels with Extended Gamut *ACS Photonics* **4** 1076–82

[88] Yang J-H, Babicheva V E, Yu M-W, Lu T-C, Lin T-R and Chen K-P 2020 Structural Colors Enabled by Lattice Resonance on Silicon Nitride Metasurfaces *ACS Nano* **14** 5678–85

[89] Zywietz U, Evlyukhin A B, Reinhardt C and Chichkov B N 2014 Laser printing of silicon nanoparticles with resonant optical electric and magnetic responses *Nat. Commun.* **5** 3402

[90] Zhu X, Yan W, Levy U, Mortensen N A and Kristensen A 2017 Resonant laser printing of structural colors on high-index dielectric metasurfaces *Sci. Adv.* **3** e1602487

[91] Okazaki T, Sugimoto H, Hinamoto T and Fujii M 2021 Color Toning of Mie Resonant Silicon Nanoparticle Color Inks *ACS Appl. Mater. Interfaces* **13** 13613–9

[92] Sheikholeslami S N, Alaeian H, Koh A L and Dionne J A 2013 A Metafluid Exhibiting Strong Optical Magnetism *Nano Lett.* **13** 4137–41

[93] Kim K, Yoo S, Huh J-H, Park Q-H and Lee S 2017 Limitations and Opportunities for Optical Metafluids To Achieve an Unnatural Refractive Index *ACS Photonics* **4** 2298–311

[94] Hinamoto T, Hotta S, Sugimoto H and Fujii M 2020 Colloidal Solutions of Silicon Nanospheres toward All-Dielectric Optical Metafluids *Nano Lett.* **20** 7737–43

